Submitted to the

Journal of Applied Physics

Evolution of the plasma composition of a high power impulse magnetron sputtering system studied with a time-of-flight spectrometer

Efim Oks
High Current Electronics Institute, Russian Academy of Sciences, 2/3 Academichesky Ave., Tomsk 634055, Russia

André Anders[*]
Lawrence Berkeley National Laboratory, 1 Cyclotron Road, Berkeley, California 94720, USA

December 31, 2008

ACKNOWLEDGMENT
This work was supported by the U.S. Department of Energy, Initiatives for Proliferation Prevention, under Contract No. DE-AC02-05CH11231 with the Lawrence Berkeley National Laboratory.

[*] Author to whom correspondence should be submitted. Electronic mail aanders@lbl.gov

Evolution of the plasma composition of a high power impulse magnetron sputtering system studied with a time-of-flight spectrometer

Efim Oks

High Current Electronics Institute, Russian Academy of Sciences, 2/3 Academichesky Ave., Tomsk 634055, Russia

André Anders*

Lawrence Berkeley National Laboratory, 1 Cyclotron Road, Berkeley, California 94720, USA

ABSTRACT

The plasma of a high power impulse magnetron sputtering (HiPIMS) system has been investigated using a time-of-flight (TOF) spectrometer. The target materials included high sputter yield materials (Cu, Ag), transition metals (Nb, Cr, Ti), and carbon (graphite); the sputtering gases were argon, krypton and nitrogen, and two different target thicknesses were selected to consider the role of the magnetic field strength. Measurements for selected combinations of those parameters give quantitative information on the transition from gas-dominated to metal-dominated (self-sputtering) plasma, on the fractions of ion charge states, and in the case of molecular gases, on the fraction of atomic and molecular ions.

PACS: 52.40.Hf, 52.25.Jm, 52.80.Tn, 81.15.Cd

* Author to whom correspondence should be submitted. Electronic mail aanders@lbl.gov

I. INTRODUCTION

High power impulse magnetron sputtering (HiPIMS) is an emerging coatings technology that recently generated a flurry of activities in terms of plasma diagnostics,[1-4] interpretation of magnetron processes under high power load conditions,[5-10] and material studies based on the effects the ionized species have on films and coatings.[11-13] By now it is well established that a large fraction of the sputtered atoms becomes ionized and participates in the sputtering process (self-sputtering[6,14-17]) by raising the peak power density by typically 2 orders of magnitude above the average value.[18,19] It has been demonstrated that the role of self-sputtering evolves as the pulse develops, however, the details of this evolution strongly depend on the target material. The evolution is also affected by the magnetic field strength on and near the target, the applied voltage, current density (power density), the features of the electric circuit, the pulse repetition rate (assisting effect of the previous pulse), and the kind and pressure of the process gas. Given the number of parameters, it is desirable to probe deeper in selected cases thereby contributing to a better understanding of processes, with the ultimate goal to improve films and coatings using this technology.

The evolution of metal species (atoms, ions) in the plasma has been demonstrated using optical emission spectroscopy[1] (OES), optical absorption spectroscopy[4] (OAS) and particle spectrometry[3,20] using so-called plasma analyzers, which are combined energy and mass spectrometers. Such methods are powerful but have limitations, for example, the optical intensity used by OES is a convolution of the density of radiating particles and their excitation conditions, and interpreting the signal height of different species in plasma analyzers is based on certain assumptions for particle transmission and detector efficiency. Therefore, it is desirable to use another, independent technique, and especially one that can give precise, time-resolved ratios between the various plasma particles.

Time-of-flight (TOF) spectrometry is such technique. It has the advantage that it can give time-resolved results by precisely delaying the gate with respect to the beginning of a plasma pulse. Such TOF system has been extensively used to study the evolution of pulsed vacuum sparks[21] and vacuum arcs.[22,23] Therefore it seems straight forward to expand the use of the TOF technique to HiPIMS pulses. In this contribution, we will demonstrate that the TOF technique can be applied to HiPIMS; we will utilize the approach to investigate the speed of metal plasma formation and gas replacement, i.e. what types of ions are present as a function of various parameters during the HiPIMS pulse evolution.

II. EXPERIMENTAL

TOF spectrometry can be done by extracting the to-be-analyzed ions from the plasma through an extractor system, such as a single hole of Pierce geometry or through a multiple hole grid system.[24,25] The accelerated ions fly to a gate system, which in our case consists of a set of annular rings;[26] in fact, we utilize the very same vacuum chamber and spectrometer previously used for pulsed vacuum sparks[21] and vacuum arcs.[22] At the gate, a short "slice" of the beam is deflected and travels to a Faraday cup detector located 1.03 m from the gate. During travel, the slice "disintegrates" and forms sub-slices of ions, each with its own mass/charge ratio, because ions with different m/q extracted with the same voltage have different velocities and arrive at the detector at different times, as indicated in Fig. 1. The time resolution is mainly limited by the duration of the TOF gate pulse, which is 200 ns.

From the Child-Langmuir law[24] it is known that a necessary condition for beam formation with reasonably high ion current is to use a high extraction voltage, which was selected to be 30 kV. Since the space-charge-compensated ion beam should be near ground potential, the plasma generator, a 2-inch (5 cm diameter) magnetron, including its power supply, must be shifted from ground to the high potential. We decided to use a pulse-forming

network (PFN) as the HiPIMS power supply in this study because this type of supply is sometimes used by other groups and it could readily be shifted to 30 kV and incorporated with the existing spectrometer. In contrast to previous HiPIMS investigations in our group,[6,10,27] where we used a "stiff" constant-voltage pulser, the voltage between target and anode is here *not* constant but depends on the impedance of the discharge. Besides the ease of design and use, PFN supplies are robust and may provide advantages in handling plasma instabilities.

The impedance of the PFN was 3 Ω and designed for a pulse duration of about 250 μs in the impedance-matched case, i.e., PFN impedance equals plasma load impedance. The pulse repetition frequency was only 1 pulse per second due to target cooling constrains. The timing was controlled via a thyristor switch (Fig. 1). Ignition of the discharge pulse at such low pulse rates is not trivial due to the missing support by the afterglow plasma from the previous pulse. Therefore, two measures were used to improve pulse ignition. First, the PFN was usually charged to its maximum of 1000 V, which helped ignition as well as ensured consistent and comparable data. Second, a bypass resistor of 2 kΩ was implemented in the circuit to ensure that the thyristor switched to the "on" condition even as the plasma was not yet ignited. To make sure that the pulse terminates and the thyristor switches "off", i.e. to avoid DC operation fed by the charging current, the charging current was limited by a resistor of 11 kΩ. All of those details are indicated in Fig. 1.

A PFN power supply provides a rectangular current pulse if the impedance of the plasma load is equal or smaller than the impedance of the PFN itself. In many cases, however, the plasma load impedance is large and variable; and therefore the current and discharge voltage will change as a function of the plasma impedance. We stress that the charging voltage (before the pulse starts) and the discharge voltage (measured between target and anode) should be not be confused. The charging voltage is externally set and a means to

influence the current, while the discharge voltage is self-adjusting and directly influences the kinetic energy of ions impacting the target.

Current and discharge voltage were monitored by a broadband inductive probe (Pearson) and by a 100:1 voltage divider (Tektronix), respectively. All electrical signals, including TOF gate and Faraday cup current, were recorded by a fast digital oscilloscope (Tektronix TDS 5054B) and exported to a personal computer for further evaluation.

The surface of the magnetron target was positioned 1 cm from the ion extraction grid of the spectrometer (Fig. 1). This distance was far enough to allow the magnetron discharge to operate yet it was close to capture the ion composition close to the location where most ions are generated. A feedback of the grid on the discharge cannot be excluded but it is believed to be of no major consequence.

A major concern for the TOF technique is that, one the one hand, enough gas is present near the target for the sputtering process to occur, yet, on the other hand, collisions of extracted ions with background gas are kept to a minimum in the time-of-flight path to the detector. Clearly, a compromise has to be made, and the only way to satisfy both requirements is to employ differential pumping. Therefore, gas was injected near the target and the extractor grid was used as low conductance element for gas flow. The main chamber, where the TOF spectrometer was housed, was pumped with a cryogenic pump (CTI, 1500 l/s). The extraction grid system consisted of three well-aligned grids (the typical acceleration-deceleration configuration) with a geometric transmittance of 55%. Differential pumping was optimized by blocking 75% of the plasma-facing grid with a stainless steel foil. The ion current to the Faraday cup was of course reduced by this blocking yet it still gave a comfortable signal-to-noise ratio, as evident by the results shown later. Via differential pumping it was ensured that the pressure in the main chamber was about 0.01 Pa or less,

while the pressure in the magnetron region was about 0.2 Pa or less. Most experiments were done with argon, but some were repeated with krypton or nitrogen.

The target materials included copper, silver, niobium, chromium, titanium, and carbon (graphite) with target thicknesses of ¼ inch (6.25 mm) or 1/8 inch (3.125 mm). The target thickness is important because it greatly affects the available magnetic induction on the surface: $B_{\|} \approx 90$ mT for the thinner target compared to $B_{\|} \approx 60$ mT for the thicker, as measured with a Hall probe in the race track region. As we will see, lower magnetic field leads to higher discharge voltage for a given current, which in turn leads to higher sputter yield but also to a greater likelihood of arcing. As the target is consumed by sputtering, one can notice a gradual shift of the current-voltage relation due to the increased magnetic field.

III. RESULTS

A. Thin copper target

It is well known that copper has one of the highest sputter yields and hence self-sputtering is most readily obtained; and therefore we will consider copper first. The ionization of sputtered atoms is particularly effective at high magnetic field strength, in our case corresponding to a thinner target.

When using the pulse-forming network, the current-voltage-time relationships are different from those previously observed with a constant voltage pulse power supply[6] because the impedance of the plasma load plays an important role on the voltage distribution and resulting current pulse. Fig. 2 shows an example for the thin, nominally 1/8 inch thick target: the voltage is noisy as long when the current is less than about 30 A; this is true at the beginning and end of each pulse.

The TOF measurements showed that the plasma composition is dominated by argon ions at the beginning of each pulse, but the copper fraction increases rapidly within the first

100 μs to reach about 80% when the maximum current is limited to 10 A and even 95% when the discharge current is as high as 60 A. Figure 3 illustrates this development by showing two extremes: an early plasma composition (20 μs after pulse begin) at relatively small discharge current (10 A, noisy voltage), and when the pulse approaches steady-state (125 μs after pulse begin) and higher discharge current (60 A, smooth voltage). The very high copper content in the latter case proves the expected dominance of self-sputtering. The plasma is dominated by singly charged ions; doubly charged copper ions, and a very small fraction of doubly charged argon ions can be observed.

Considering the steady-state part of the current-voltage-time characteristics, e.g. about 125 μs after the beginning of each pulse, one can construct a current-voltage relationship free of time, which turns out to be non-monotonic (Fig. 4). Interestingly, the minimum voltage coincides with the threshold current beyond which the noise of the voltage disappears, which will be further discussed in section IV.

One would expect that as the PFN is charged to higher voltages, driving higher current and power, more copper is provided, and the fraction of argon decreases. This is indeed the case, as shown in Fig. 5. One can see that at the relatively low current of 10 A, the copper fraction decreases at the end of the pulse. For higher currents, however, no such reduction is observed anymore.

While the sputter yield depends on both the target material and kind of gas, copper can be effectively sputtered with gases other than argon. For example, even a molecular gas like nitrogen can be used. One will find both molecular and atomic gas ions in the plasma. The results of Fig. 6 show that the atomic fraction (N^+) is remarkably high despite the strong triple bond of the nitrogen molecule. This is another indication for the presence of energetic electrons and a high collision frequency. As with argon, the nitrogen gas is quickly replaced by copper during the HiPIMS pulse, and self-sputtering takes over.

B. Thick copper target

As mentioned in section II, the thicker copper target (1/4 inch = 6.25 mm) leads to a much weaker magnetic induction on and above the surface of the target. To obtain the same discharge current for the same given pressure, a higher discharge voltage is needed, which leads to a higher energy of ions bombarding the target. Therefore, a thicker target implies greater power input and higher energy of bombarding ions *if we consider the case of equal currents*. Fig. 7 shows an example of the voltage enhancement for a current of 40 A (this nominal current refers to the steady-state value). One should note that while the thinner target shows the characteristic noise when the current is less than 30 A, no such noise can be seen with the thicker target.

C. Silver

Like copper, silver has a very high sputtering yield, and therefore one would expect a behavior similar to copper. Indeed, this is the case and therefore we can be brief in this section. The discharge turned out to be of higher impendence, which increased throughout the pulse, and hence the current was decreasing (Fig. 8). Yet, the metal content increased quickly at the beginning of each pulse and reached steady-state. In analogy to Fig. 6 for copper, we show this behavior when using nitrogen as the sputter gas (Fig. 8); it is remarkable how stable the plasma composition is despite the diminishing current and power level. We state that Ag^{2+} ions were recorded, too, however only at a level of about 1% and therefore not shown in Fig. 8.

D. Niobium

Going to target materials with smaller sputtering yield, quite remarkable changes are observed that sensitively depend on the target material and gas type. Strong differences can also be found when using thicker targets, i.e. effectively lower magnetic field, which requires higher voltage (and power) considering the case of approximately equal current in the steady-state portion of the pulse. The voltage and current for a thinner target are much noisier than when the thicker target is used. For example, to obtain a steady-state current of 30 A with argon at 0.05 Pa, established after about 50 μs, the discharge voltage is noisy 600 V for the thin (3.125 mm) target, and smooth 800 V for the thick (6.25 mm) target. The corresponding power in the steady-state phase is 18 kW and 24 kW, respectively, or expressed as power density averaged over the whole target, approximately 0.9 kW/cm^2 and 1.2 kW/cm^2, respectively. The plasma composition is quite different for those cases: it remained to be dominated by argon gas ions for the thinner target, whereas the niobium fraction is much higher for the thicker target (Fig 9). Compared to copper and silver, the fraction of doubly charged ions is much higher, although singly charged ions still dominate the plasma.

Using a molecular gas such as nitrogen, we find again a very strong dissociation of the gas to the point when atomic gas ions (N^+) are more frequent than molecular ions (N_2^+). Figure 10 shows the compilation of the niobium-nitrogen measurements. Note that for the ticker target, in contrast to the results with argon (Fig. 9), the impedance of the discharge increases, and therefore the niobium fraction does not reach steady-state but keeps adjusting throughout the discharge pulse.

E. Chromium

Discharges with chromium are qualitatively similar to the previous case of niobium. Fig. 11 shows the more interesting case of a thicker target (6.25 mm) when using argon or nitrogen as the discharge gas. However, the impedance and hence the plasma composition

did not really reach any steady-state during each pulse, rather, the current kept falling; the metal content increases during most of the pulse until, near the end of the pulse, the metal fraction starts to decline. The metal fraction was much higher for the case of argon, even as the current was much lower than for the nitrogen case. The charging voltage was always the same, and we should keep in mind that lower current means higher impedance and greater discharge voltage. The voltage was much noisier for nitrogen than for argon (not shown) and we notice the very strong dissociation and ionization of the gas molecules, leading to the dominance of N^+ ions.

The series of experiments with chromium was completed using krypton as the discharge gas. The discharge voltage was slightly higher than in the case of argon, but the overall behavior was similar and therefore we do not further elaborate on this case.

F. Titanium

Titanium was the third transition metal investigated; it shows in many respects a qualitatively similar behavior to Nb and Cr. For the thinner target (3.125 mm), the impedance of the discharge was low and approximately matched the impedance of the PDF. Therefore the pulse shape was more rectangular as we are used to from pulsed arc experiments, yet, the discharge voltage level of 550 V – 600 V proves that the discharge is not an arc. The discharge voltage was always noisy, especially when the discharge was pushed to the lowest possible pressure of about 0.04 Pa.

Switching to krypton causes the discharge voltage to significantly increase by about 120 V compared to argon, namely from 550 V to 670 V in the steady-state portion of the pulse. As a consequence, the ion charge states shift to higher values. Interestingly, as shown in Fig. 12, there is evidence for charge states higher than 2+, however, the resolution is insufficient to resolve isotopes and therefore one cannot conclusively determine the

contributions of contamination. The mass/charge ratio of the following species is the same: $m/q = 28$ for Kr^{3+} and N_2^+, $m/q = 16$ for Ti^{3+} and O^+, and $m/q = 12$ for Ti^{4+} and C^+. Based on the contamination level for other measurements, and the height of the signals, one can assume that at least part of the signal is caused by Kr^{3+}, Ti^{3+} and Ti^{4+}.

G. Carbon

The experiments are concluded here by considering a target made from graphite, a semimetal that is know for its very low self-sputtering yield (always less than unity). The impedance of the discharge with argon at 0.04 Pa is relatively low, giving an approximately rectangular current pulse of 70 A in the steady-state portion. The TOF ion spectrum indicates that Ar^+ ions are initially dominant, but those gas ions are soon surpassed by C^+ ions. Small amounts (~ 1%) of C^{2+} can be detected, too, besides Ar^{2+} and contaminations such as hydrogen, oxygen, and nitrogen.

IV. DISCUSSION

A. General

In the present study of HiPIMS discharges, several process parameters were varied, including target material, the kind and pressure of process gas, and the magnetic field strength (via target thickness). As a consequence of using a PFN and various process parameters, the impedance became a variable, too, leading to different currents and discharge voltages, the latter in turn directly affected the energy of ions impacting the target, which in turn affected the sputtering yield. Therefore, we have explored a large variety of conditions which required us to make a reasonable selection (limitation) of combinations.

B. Power Supply Effects

The use of a PFN power supply, while convenient in practical cases like ours, leads to plasma conditions that are much more difficult to interpret than when a stiff, constant-voltage power supply is employed. For a constant voltage supply, we have thoroughly demonstrated earlier[6,7,27,28] that self-sputtering can run away to reach a new steady-state; the amplification (run-away) can occur abruptly when the condition $\Pi \equiv \alpha\beta\gamma_{SS} > 1$ is reached[29]; here α is the probability that a sputtered atom is ionized, β is the probability that this newly formed ion returns to the target, and γ_{SS} is the self-sputtering yield, which depends on the target material and on the energy of the impacting ion. In the case of a PFN as the power supply, the current is determined by the charging voltage and the combined impedance of the supply and the load. The load impedance often exceeds the PFN impedance, and therefore the current and discharge voltage are not constant during the pulse. We could have designed the PFN with a higher impedance to obtain a more constant current, however, that would have implied using a very high charging voltage (> 1 kV) or to accept relatively modest currents, which is contrary to our desire to clearly operate in the HiPIMS regime. Therefore the first main conclusion is that PFN power supplies do not only make it difficult to compare physical results but they are less suitable to reach the desirable high power level for HiPIMS (on a second thought, this "soft" load feedback behavior may be beneficial in suppressing plasma instabilities – a subject to be explored further). With the given PFN, selfsputtering runaway ($\Pi > 1$) and transition to sustained self-sputtering ($\Pi = 1$) is more subtle and gradual, and in some cases does not occur.

C. Copper and Silver

Copper and silver were chosen due to their exceptionally high self-sputter yield; it is well established that sustained self-sputtering can be done even without gas in DC,[15,29]

medium frequency[17] and HiPIMS modes.[27,28] The discharge pulse is characterized by a relatively long initial phase towards steady-state (Fig. 2), indicative of self-sputtering replacing gas sputtering. With a stiff power supply, this process occurs rapidly,[6,7] here, however, an increase in current is accompanied by a decrease in discharge voltage, thus slowing the transition (left branch of Fig. 4, which can be associated with the initial phase of each discharge pulse). Figures 3 and 5 prove that metal ions have replaced most of the gas ions in the sputtering process.

The flat portion of the current-voltage-time characteristic indicates the establishment of a steady-state situation, which is reached after 120 μs for copper (Figs. 2, 6 and 7). The measurement of the plasma evolution (Fig. 5) supports this interpretation: the fraction of metal is about constant about 120 μs after the start of a discharge pulse.

Reaching steady-state within the limited pulse length is not always a given: even silver, a similar material, shows a declining current (Fig. 8). Steady-state implies establishment of the $\Pi = 1$ condition which implies settling of the electron temperature and "loss" pathways for sputtered atoms. The system is generally stabilized via the electron temperature. Suppose more atoms are sputtered by a fluctuation spike of ions impacting the target, those additional atoms will lead to greater cooling electrons, and thus fewer ions are produced, counteracting the original spike in the ion flux. A detailed model of those processes remains to be developed.

To illustrate the difficulties for this modeling, we should look at Fig. 4 showing the current-voltage relationships in the middle of the pulse: The falling part of the curve, at low currents, is indicative that the plasma is more heated and the rarefaction effect[30-32] becomes stronger with increasing current, whereas the rising part, at high currents, indicates that self-sputtering of metal has taken over the process. The approximately ohmic behavior, i.e. linear current-voltage relation, is most likely caused by the increasingly high density of sputtered

metal atoms and the collisions caused by them (recall that ohmic behavior is related to collisions and cooling of charge carriers).

Driving the discharge "harder" by selecting higher charging voltage (Fig. 5) leads to higher discharge currents and faster replacement of gas ions by metal ions. As indicated by the minimum in the curve of Fig. 4, the character of the discharge is changed when the discharge is has reached the 40 A level. Related, once the discharge operates with 40 A, the plasma is already dominated by metal and further enhancement of the current does not change this fact anymore (Fig. 5).

Changing the gas from argon to nitrogen has an influence only on the initial phase of each pulse when gas ions are still important. In later phases of the discharge pulse, self-sputtering is dominant. For example, comparing sputtering with argon (Fig. 5) and nitrogen (Fig. 6), and considering the case of 40 A of discharge current in the steady-state phase, we find that 95% of ions are Cu^+ in both cases. Consistent with the notion of low electron temperature in the case of sustain self-sputtering of copper, nitrogen ions are predominantly molecular (Fig. 6).

The use of a thinner target means that the magnetic field is stronger on and near the target surface; this will better confine energetic secondary electrons, enhances near target ionization, increases the current, and reduces the discharge voltage. Conversely, a thicker target means lower field, less ionization, less current unless we consider cases where the current is adjusted to be the same as with the thinner target. This adjustment is done using higher charging voltage, and as a consequence of comparing equal current situations, the discharge voltage driving the processes is higher for the thicker target (Fig. 7). By "driving" we mean the acceleration of ions towards the target, and of secondary electrons away from the target. Both processes are critical to the operation of the magnetron discharge, the former causing sputtering, the latter ionization and heating of the plasma. Due to the adjustment of

the charging voltage to get equal currents, the thicker target is operated by higher power density and therefore shows more readily the characteristics of HiPIMS.

D. Transition metals niobium, chromium, and titanium

The transition metals have a much smaller sputtering yield, leading to lower density of sputtered atoms and higher electron temperature. Fewer sputtered atoms also imply that metal-sustained self-sputtering, where $\Pi = 1$, is not easily achieved. Therefore, the contribution of gas ions remains high, and the influence of the gas is much more important than for the cases of copper and silver.

The niobium plasma composition at different target thickness (Fig. 9) is consistent with the interpretation given at the end of the last sub-section. Here, however, the higher power density for the thicker target leads to not only higher metal content but to a significant enhancement of the fraction of doubly charged ions. Those doubly charged ions have a much higher yield of secondary electrons,[9,33] which in turn allow for high plasma electron temperature and enhanced ionization.

When nitrogen is used as sputtering gas (Fig. 10), the sputtering yield is much lower due to the lower mass of nitrogen and the effective half of the kinetic energy per nitrogen atom when molecular ions are impacting. Comparing the two different target thicknesses for approximately equal currents in the middle of the pulse, we see that the thicker target is being driven by higher initial current (higher charging voltage, as discussed before). This leads to higher metal content in the plasma, enhanced nitrogen dissociation, and a greater fraction of atomic nitrogen ions (Fig. 10 bottom) compared to the case of a thinner target (Fig. 10 top).

Figure 11 provides a direct comparison of the gas effect using the thicker chromium target. Again, argon is has a higher sputtering yield, leading to dominance of the metal content in the plasma compared to when using nitrogen. Yet, the sputtering yield is much

lower than with copper, and therefore electrons are less cooled, compared to copper, and the nitrogen is more efficiently dissociated and ionized.

Looking at Fig. 12, which shows the case of titanium, the electron temperature seems to be even higher since there is evidence of higher charge states. Those measurements support recent measurements done with a different discharge system using an electrostatic plasma analyzer,[10] however, our TOF measurements are not conclusive as already indicated in the experimental section.

E. Carbon

The measurements were concluded by considering carbon. Sputtering of carbon has been an extensive field of research mainly with the goal to synthesize hard and protective diamond-like carbon (DLC) coatings. Sputtering can be done in argon, leading to amorphous carbon (a-C) films, or in a argon/hydrogen gas, to hydrogenate the film (a-C:H), or in argon/nitrogen to obtain nitrided amorphous carbon, a-C:N, which is of importance to hard disk in the magnetic information storage industry. Previous attempts to improve the quality of sputtered DLC using HiPIMS technology remained inconclusive[34] and here we considered only what the carbon ion fraction in such discharge pulses is because only ionized carbon can be controlled by biasing to make films of desired quality. As shown in Fig. 12, the carbon ion fraction is surprisingly high, given the small self-sputtering yield of carbon (less than 0.4 for all energies, see Fig. 16 of ref.[6]). Therefore, the quest for improved sputtered DLC films is still meaningful.

V. CONCLUSIONS

Current-voltage-time characteristics showed that the use of a pulse-forming network (PFN) is less desirable than a “stiff” constant voltage supply because, from a physics

interpretation point of view, the discharge voltage is not constant and therefore the energy of ions impacting the target changes. This affects the sputtering yield of ions impacting the target, and it is therefore also not desirable from a control and practical implementation point of view.

The TOF measurements of the plasma composition of HiPIMS discharges indicated strong differences between the target materials which are also affected by the type and pressure of the gas, the current and voltage level, time in the pulse, and strength of the magnetic field. Selected examples of parameter combinations supported the previous findings that the plasma composition changes from being gas-ion-dominated to metal-ion-dominated. For materials with high sputtering yield, like copper and silver, the change occurs relatively quickly (~ 100 μs) and completely, so that the type of gas becomes irrelevant later in the pulse.

For target materials of lower sputtering yield, like transition metals, the transition to metal plasma is not as complete. Electrons are less cooled in those cases, and large fractions of doubly charged ions appear, especially with argon or krypton. With nitrogen, however, much energy is spent in dissociating and ionizing the gas, leading to a large fraction of N^+ ions, and less metal, which is also due to the small sputtering yield. In the case of titanium even higher charge states may be possible, but the resolution was insufficient to identify the contribution of contamination by utilizing isotope distributions.

Finally, HiPIMS of carbon leads to a large fraction of C^+ ions in the plasma, which revives hopes for the deposition of well controlled, high-quality diamond-like carbon materials made by sputtering.

ACKNOWLEDGEMENTS

This work was supported by the U.S. Department of Energy, Initiatives for

Proliferation Prevention, under Contract No. DE-AC02-05CH11231 with the Lawrence Berkeley National Laboratory.

References

[1] A. P. Ehiasarian, R. New, W.-D. Münz, L. Hultman, U. Helmersson, and V. Kouznetsov, Vacuum **65,** 147 (2002).

[2] J. Bohlmark, J. T. Gudmundsson, J. Alami, M. Lattemann, and U. Helmersson, IEEE Trans. Plasma Sci. **33,** 346 (2005).

[3] J. Bohlmark, M. Lattemann, J. T. Gudmundsson, A. P. Ehiasarian, Y. Aranda Gonzalvo, N. Brenning, and U. Helmersson, Thin Solid Films **515,** 1522 (2006).

[4] S. Konstantinidis, A. Ricard, M. Ganciu, J. P. Dauchot, C. Ranea, and M. Hecq, J. Appl. Phys. **95,** 2900 (2004).

[5] D. J. Christie, J. Vac. Sci. Technol. A **23,** 330 (2005).

[6] A. Anders, J. Andersson, and A. Ehiasarian, J. Appl. Phys. **102,** 113303 (2007).

[7] A. Anders, J. Andersson, and A. Ehiasarian, J. Appl. Phys. **103,** 039901 (2008).

[8] J. Vlček, P. Kudláček, K. Burcalová, and J. Musil, J. Vac. Sci. Technol. A **25,** 42 (2007).

[9] A. Anders, Appl. Phys. Lett. **92,** 201501 (2008).

[10] J. Andersson, A. P. Ehiasarian, and A. Anders, Appl. Phys. Lett. **93,** 071504 (2008).

[11] A. P. Ehiasarian, P. E. Hovsepian, L. Hultman, and U. Helmersson, Thin Solid Films **457,** 270 (2004).

[12] J. Alami, P. Eklund, J. M. Andersson, M. Lattemann, E. Wallin, J. Bohlmark, P. Persson, and U. Helmersson, Thin Solid Films **515,** 3434 (2007).

[13] A. P. Ehiasarian, J. G. Wen, and I. Petrov, J. Appl. Phys. **101,** 054301 (2007).

[14] N. Hosokawa, T. Tsukada, and T. Misumi, J. Vac. Sci. Technol. **14,** 143 (1977).

[15] W. M. Posadowski and Z. Radzimski, J. Vac. Sci. Technol. A **11,** 2980 (1993).

[16] W. M. Posadowski, A. Wiatrowski, J. Dora, and Z. J. Radzimski, Thin Solid Films **516,** 4478 (2008).

[17] A. Wiatrowski, W. M. Posadowski, and Z. J. Radzimski, J. Vacuum Sci. Technol. A **26,** 1277 (2008).

[18] V. Kouznetsov, K. Macak, J. M. Schneider, U. Helmersson, and I. Petrov, Surf. Coat. Technol. **122,** 290 (1999).

[19] J. Bohlmark, J. Alami, C. Christou, A. Ehiasarian, and U. Helmersson, J. Vac. Sci. Technol. A **23,** 18 (2005).

[20] J. Vlcek, A. D. Pajdarova, and J. Musil, Contrib. Plasma Phys. **44,** 426 (2003).

[21] G. Y. Yushkov and A. Anders, Appl. Phys. Lett. **92,** 041502 (2008).

[22] A. Anders and G. Y. Yushkov, J. Appl. Phys. **91,** 4824 (2002).

[23] E. Oks, G. Y. Yushkov, and A. Anders, Rev. Sci. Instrum. **79,** 02B301 (2008).

[24] A. T. Forrester, *Large Ion Beams* (Wiley, New York, 1988).

[25] *The Physics and Technology of Ion Sources*; edited by I. G. Brown (Wiley-VCH, Weinheim, 2004).

[26] I. G. Brown, J. E. Galvin, R. A. MacGill, and R. T. Wright, Rev. Sci. Instrum **58,** 1589 (1987).

[27] J. Andersson and A. Anders, Appl. Phys. Lett. **92,** 221503 (2008).

[28] J. Andersson and A. Anders, Phys. Rev. Lett.**,** accepted for publication (2009).

[29] N. Hosokawa, T. Tsukada, and H. Kitahara, *Effect of discharge current and sustained self-sputtering*, Proc. 8th Int. Vacuum Congress, Le Vide, Cannes, France, 11-14 (1980).

[30] A. Anders, J. Andersson, D. Horwat, and A. Ehiasarian, *Physics of high power impulse magnetron sputtering*, The Ninth International Symposium on Sputtering & Plasma Processes - ISSP 2007, Kanazawa, Japan, June 6-8, 2007, 195-200 (2007).

[31] S. M. Rossnagel, J. Vac. Sci. Technol. A **6,** 19 (1988).

[32] G. M. Turner, J. Vacuum Sci. Technol. A **13,** 2161 (1995).

[33] G. Laktis, F. Aumayr, and H. Winter, J. de Physique **50,** C1 (1989).

[34] B. M. DeKoven, P. R. Ward, R. E. Weiss, D. J. Christie, R. A. Scholl, W. D. Sproul, F. Tomasel, and A. Anders, *Carbon thin film deposition using high power pulsed magnetron sputtering*, 46th Annual Technical Conference of the Society of Vacuum Coaters, San Francisco, CA, Society of Vacuum Coaters, 158-165 (2003).

Figure Captions

Fig. 1 Setup and basic electric schematic of the experiment (geometric dimensions are not to scale).

Fig. 2 Example of a current and voltage pulse when using a copper target of 3.125 mm thickness with argon at a pressure of 0.05 Pa; note that the voltage is noisy when the current is less than about 30 A.

Fig. 3 Examples of two extreme TOF spectra: Top: measurement at the early time of 20 μs after pulse begin, when the discharge current is going to be limited to the relatively small value of 10 A; Bottom: measurement 125 μs after pulse begin, when the pulse has reached steady-state, here at 60 A.

Fig. 4 Current-voltage characteristic constructed using the steady-state part of the pulses, e.g. about 125 μs after the beginning of each pulse. Note that the voltages on the low current segment are noisy, whereas the voltages at currents greater than 30 A are smooth; thin copper target of nominal 3.125 mm and argon at pressure 0.05 Pa.

Fig. 5 Fraction of copper ions in the plasma as a function of time, with the maximum steady-state current as a parameter (copper target, argon pressure 0.05 Pa).

Fig. 6 Fraction of copper and nitrogen ions, both molecular and atomic, as a function of time; additionally, the current is shown here, too, reaching 42 A in the steady-state phase.

Fig. 7 Discharge voltage, as measured between target and anode, as a function of time, for a different target thicknesses but at the same current of 40 A (the steady-state value of the pulse).

Fig. 8 Evolution of the plasma composition for a thick (6.25 mm) silver target operated in nitrogen of 1 Pa.

Fig. 9 Evolution of the plasma composition during a HiPIMS discharge with a niobium target in argon; top: thin target, bottom: thick target.

Fig. 10 As figure 9 but with nitrogen as the discharge gas.

Fig. 11 Evolution of the plasma composition during a HiPIMS discharge with a chromium target in argon (top) and nitrogen (bottom).

Fig. 12 Ion current to the magnetically suppressed Faraday cup for HiPIMS discharge with a 3.125 mm thick titanium target operating in krypton at 0.04 Pa, current at steady-state 100 A; top: 25 μs after pulse start; bottom: 250 μs after pulse start.

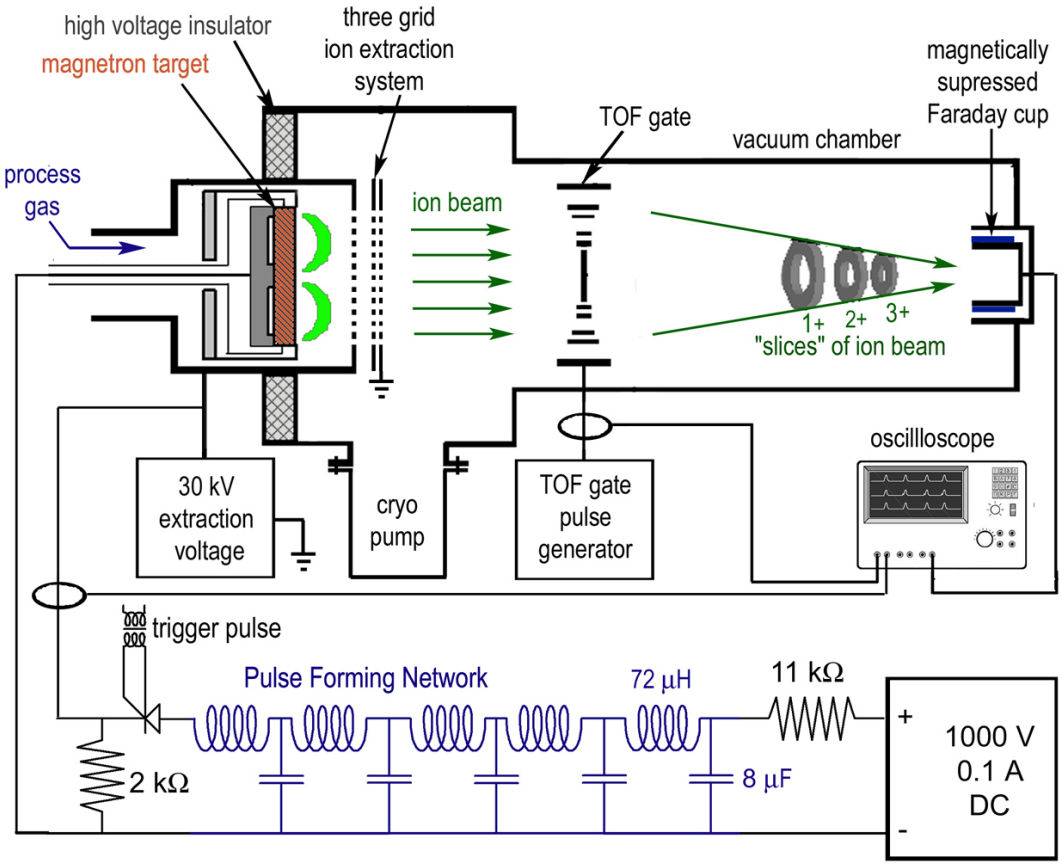
high voltage insulator
magnetron target
three grid
ion extraction
system
TOF gate
vacuum chamber
magnetically
supressed
Faraday cup
process
gas
ion beam
1+ 2+ 3+
"slices" of ion beam
oscillloscope
30 kV
extraction
voltage
cryo
pump
TOF gate
pulse
generator
trigger pulse
Pulse Forming Network
72 μH
11 kΩ
+
1000 V
0.1 A
DC
-
2 kΩ
8 μF

Fig. 1

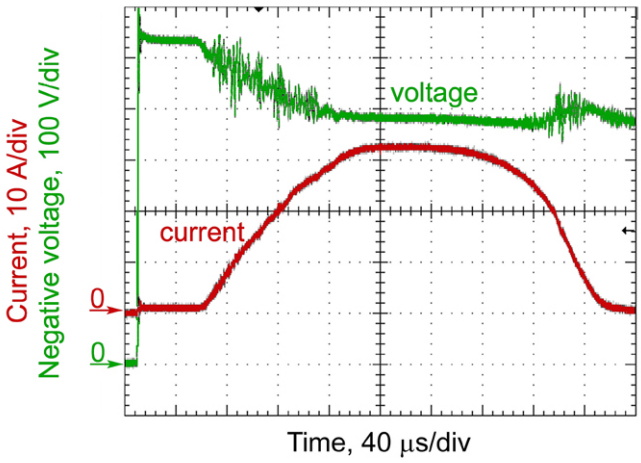
Current, 10 A/div
Negative voltage, 100 V/div
voltage
current
0
0
Time, 40 μs/div

Fig. 2

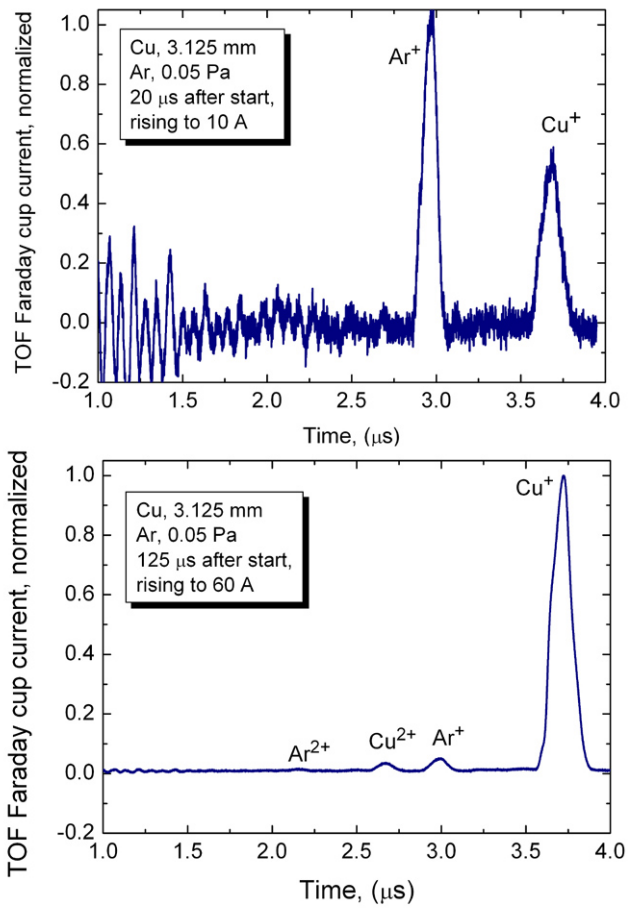
Cu, 3.125 mm
Ar, 0.05 Pa
20 μs after start,
rising to 10 A
Ar+
Cu+
TOF Faraday cup current, normalized
Time, (μs)
Cu, 3.125 mm
Ar, 0.05 Pa
125 μs after start,
rising to 60 A
Cu+
Ar2+
Cu2+
Ar+
TOF Faraday cup current, normalized
Time, (μs)

Fig. 3

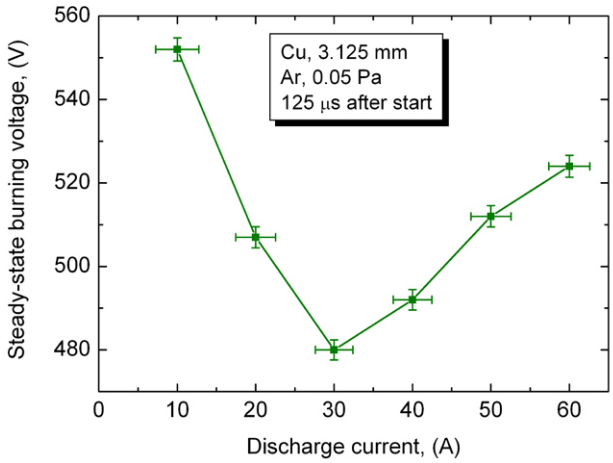
Cu, 3.125 mm
Ar, 0.05 Pa
125 μs after start
Steady-state burning voltage, (V)
Discharge current, (A)
560
540
520
500
480
0
10
20
30
40
50
60

Fig. 4

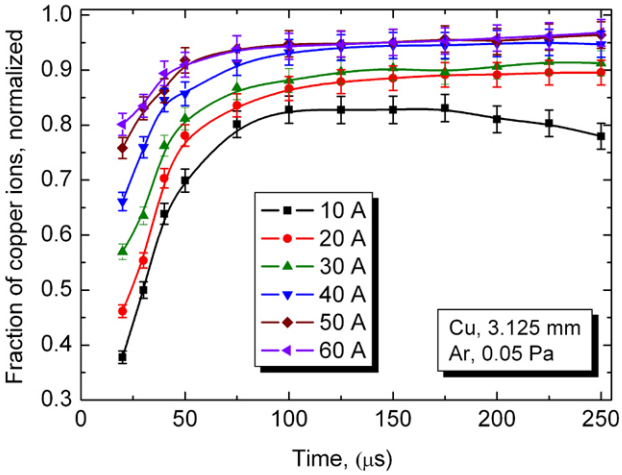
Fraction of copper ions, normalized
Time, (μs)
10 A
20 A
30 A
40 A
50 A
60 A
Cu, 3.125 mm
Ar, 0.05 Pa

Fig. 5

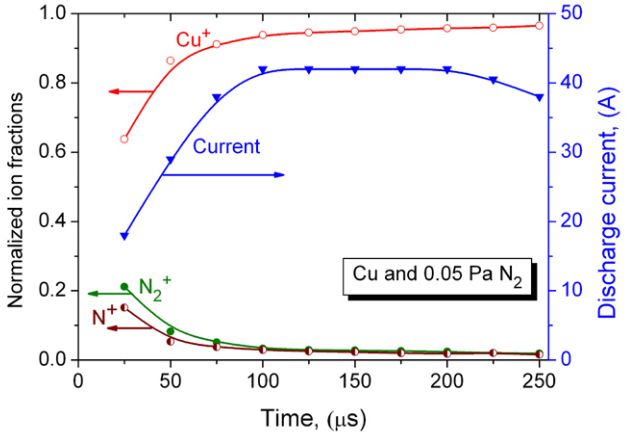
Normalized ion fractions
Discharge current, (A)
Time, (μs)
Cu+
Current
N2+
N+
Cu and 0.05 Pa N2
1.0
0.8
0.6
0.4
0.2
0.0
50
40
30
20
10
0
0
50
100
150
200
250

Fig. 6

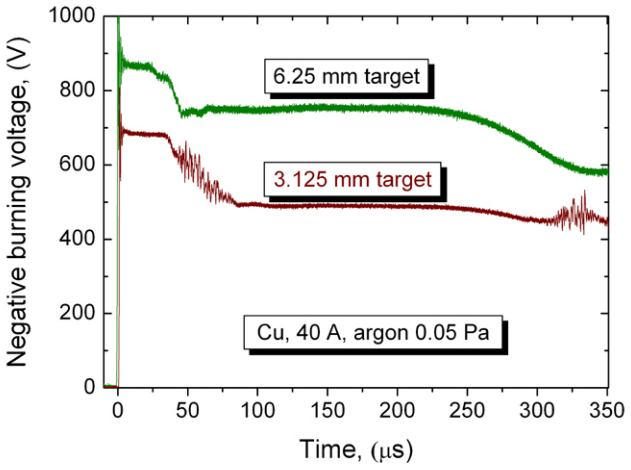
Negative burning voltage, (V)
1000
800
600
400
200
0
0
50
100
150
200
250
300
350
Time, (μs)
6.25 mm target
3.125 mm target
Cu, 40 A, argon 0.05 Pa

Fig. 7

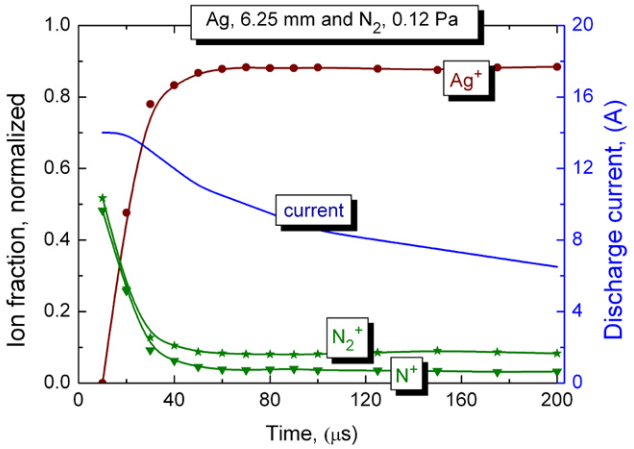
Ag, 6.25 mm and N2, 0.12 Pa
Ag+
current
N2+
N+
Ion fraction, normalized
Discharge current, (A)
Time, (μs)
1.0
0.8
0.6
0.4
0.2
0.0
20
16
12
8
4
0
0
40
80
120
160
200

Fig.8

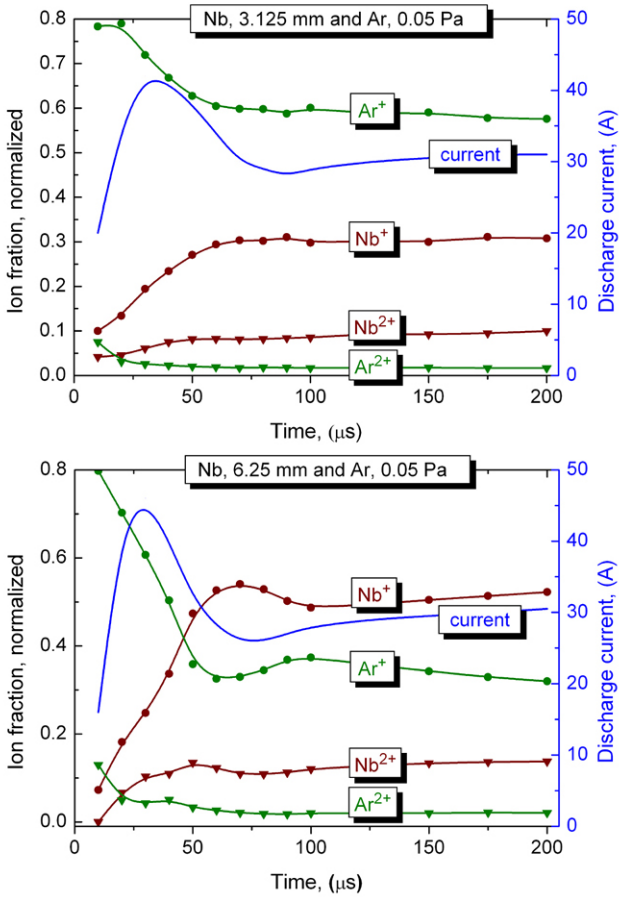
Nb, 3.125 mm and Ar, 0.05 Pa
Ar+
current
Nb+
Nb2+
Ar2+
Ion fration, normalized
Discharge current, (A)
Time, (μs)
Nb, 6.25 mm and Ar, 0.05 Pa
Nb+
current
Ar+
Nb2+
Ar2+
Ion fraction, normalized
Discharge current, (A)
Time, (μs)

Fig. 9

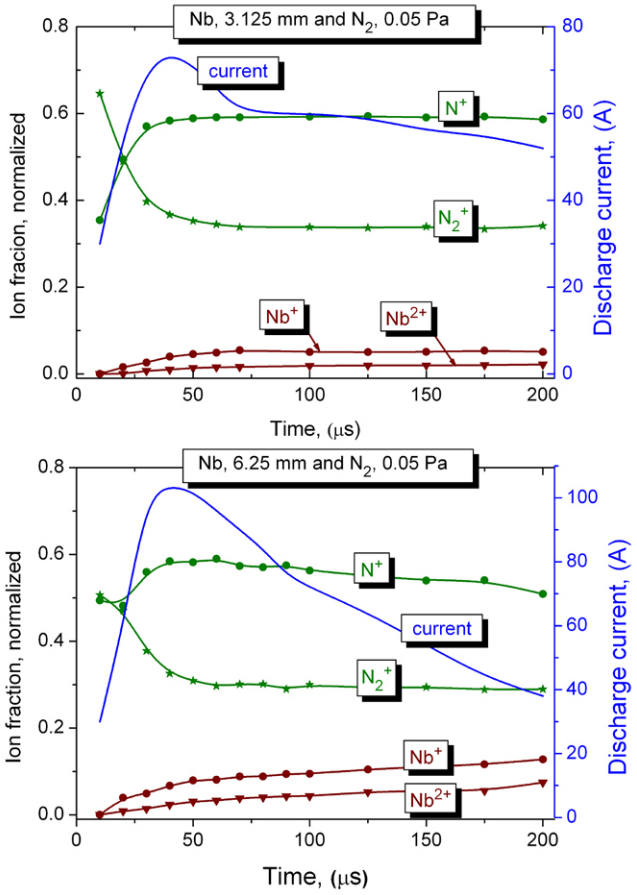
Nb, 3.125 mm and N2, 0.05 Pa
current
N+
N2+
Nb+
Nb2+
Ion fracion, normalized
Discharge current, (A)
Time, (μs)
Nb, 6.25 mm and N2, 0.05 Pa
current
N+
N2+
Nb+
Nb2+
Ion fraction, normalized
Discharge current, (A)
Time, (μs)

Fig. 10

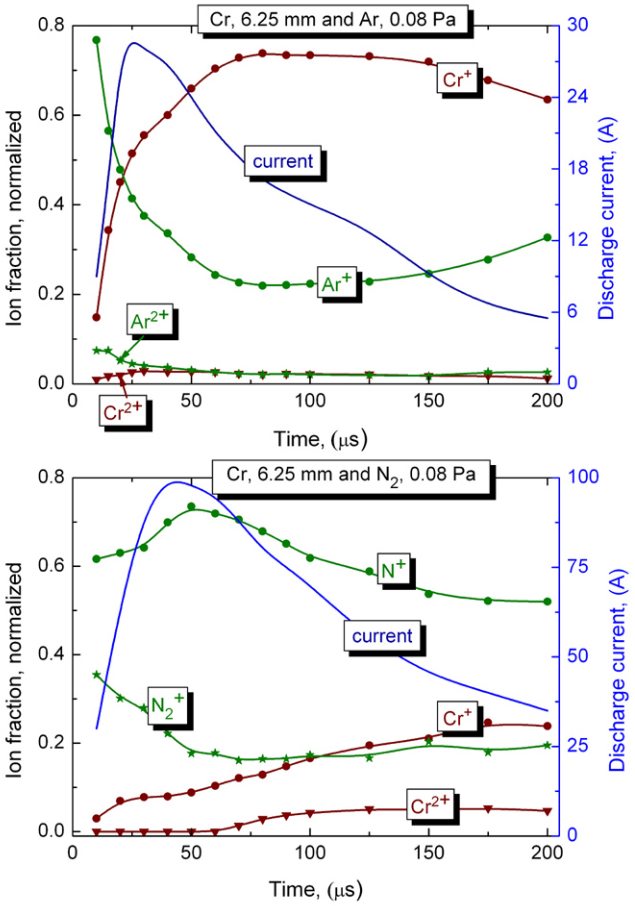
Cr, 6.25 mm and Ar, 0.08 Pa
Ion fraction, normalized
Discharge current, (A)
Time, (μs)
Cr+
current
Ar+
Ar2+
Cr2+
Cr, 6.25 mm and N2, 0.08 Pa
N+
current
N2+
Cr+
Cr2+

Fig. 11

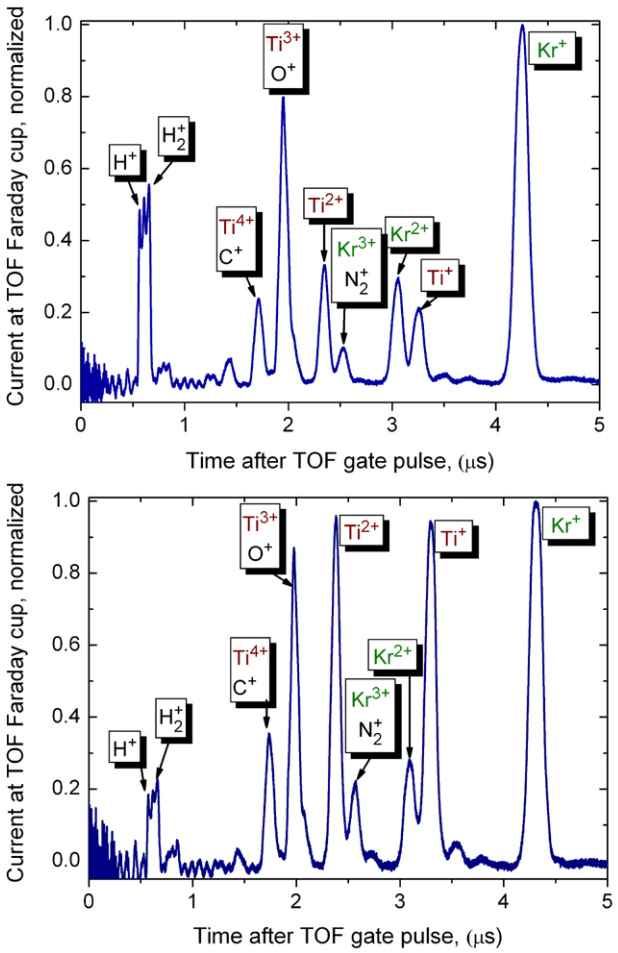
Current at TOF Faraday cup, normalized
Time after TOF gate pulse, (μs)
H+
H2+
Ti4+ C+
Ti3+ O+
Ti2+
Kr3+ N2+
Kr2+
Ti+
Kr+

Fig. 12